

## High-Adiabat High-Foot Inertial Confinement Fusion Implosion Experiments on the National Ignition Facility

H.-S. Park,<sup>\*</sup> O. A. Hurricane,<sup>†</sup> D. A. Callahan, D. T. Casey, E. L. Dewald, T. R. Dittrich, T. Döppner, D. E. Hinkel, L. F. Berzak Hopkins, S. Le Pape, T. Ma, P. K. Patel, B. A. Remington, H. F. Robey, and J. D. Salmonson  
*Lawrence Livermore National Laboratory, P.O. Box 808, Livermore, California 94551, USA*

J. L. Kline

*Los Alamos National Laboratory, P.O. Box 1663, Los Alamos, New Mexico 87545, USA*

(Received 14 October 2013; published 5 February 2014)

This Letter reports on a series of high-adiabat implosions of cryogenic layered deuterium-tritium (DT) capsules indirectly driven by a “high-foot” laser drive pulse at the National Ignition Facility. High-foot implosions have high ablation velocities and large density gradient scale lengths and are more resistant to ablation-front Rayleigh-Taylor instability induced mixing of ablator material into the DT hot spot. Indeed, the observed hot spot mix in these implosions was low and the measured neutron yields were typically 50% (or higher) of the yields predicted by simulation. On one high performing shot (N130812), 1.7 MJ of laser energy at a peak power of 350 TW was used to obtain a peak hohlraum radiation temperature of  $\sim 300$  eV. The resulting experimental neutron yield was  $(2.4 \pm 0.05) \times 10^{15}$  DT, the fuel  $\rho R$  was  $(0.86 \pm 0.063)$  g/cm<sup>2</sup>, and the measured  $T_{\text{ion}}$  was  $(4.2 \pm 0.16)$  keV, corresponding to 8 kJ of fusion yield, with  $\sim 1/3$  of the yield caused by self-heating of the fuel by  $\alpha$  particles emitted in the initial reactions. The generalized Lawson criteria, an ignition metric, was 0.43 and the neutron yield was  $\sim 70\%$  of the value predicted by simulations that include  $\alpha$ -particle self-heating.

DOI: [10.1103/PhysRevLett.112.055001](https://doi.org/10.1103/PhysRevLett.112.055001)

PACS numbers: 52.57.Fg, 52.70.La, 52.70.Nc

To achieve ignition in inertial confinement fusion (ICF) experiments at the National Ignition Facility (NIF) [1] requires that the deuterium-tritium (DT) fuel be compressed to 1000 g/cm<sup>3</sup> and the central hot spot heated to  $T_{\text{ion}} \sim 10$  keV. In this hot spot ignition scheme, the hot spot ignites with much lower DT density. Once the hot spot ignites, burn will then propagate into the fuel if and only if the fuel is sufficiently dense. To make maximum use of available laser energy, the DT fuel in imploding ignition capsules is kept in a nearly Fermi degenerate state by driving the fuel along a low-entropy trajectory in pressure-density space characterized by low values of the adiabat. Here, the adiabat is defined as  $\alpha = P/P_{\text{cold}}$ , ( $P/P_{\text{Fermi}}$  is an alternate and more commonly used definition) where  $P$  is the mass averaged DT fuel pressure at peak velocity, and  $P_{\text{cold}}$  is the minimum pressure at 1000 g/cm<sup>3</sup> which is very close to the ideal Fermi degenerate pressure for DT [2]. Previous experiments at NIF used a weak first laser pulse (the “picket”), a “low foot,” followed by three subsequent pulses whose timing and level are adjusted to drive the fuel along a low adiabat ( $\alpha \sim 1.5$ ) [3]. These experiments achieved high implosion velocities and high DT fuel areal densities,  $\rho R$ , but the measured yields do not compare favorably with the predictions of 1D “clean” simulations. The best performing low-adiabat implosion to date achieved a neutron yield of  $7.5 \times 10^{14}$  neutrons with a fuel areal density of  $\rho R \sim 1.3$  g/cm<sup>2</sup>; but typical values for the measured yield

over simulation predictions of yield (YOC) for low-adiabat implosions are only 3%–25% [4].

The Rayleigh-Taylor (RT) and Richtmyer-Meshkov (RM) instabilities [5] can cause capsule surface and interface imperfections to grow and if severe enough, the instabilities can cause ablator material to mix into the core and radiatively cool the hot spot, decreasing the hot spot temperature and nuclear yield. Low-adiabat implosions are more susceptible to these instabilities; this may explain their lower than predicted performance. High-foot high-adiabat implosions reduce the ablation front RM and RT growth [6] resulting in measured performance closer to predicted performance (at the expense of requiring more laser energy to achieve the required fuel density for ignition). The in-flight aspect ratio for the high-foot implosion is roughly half that of the low-foot implosion throughout most of the implosion. This means the thickness of the ablator (and associated density scale height) for the high foot is roughly twice that of the low foot (the effect of higher adiabat). This reduces the unstable RT drive in the high foot as compared to the low foot. Enhanced ablative stabilization is also present in the high foot due to the higher  $T_{\text{rad}}$  (radiation temperature) at early times (the effect of higher foot temperature). These details and the tradeoffs are discussed in the companion Letter by Dittrich *et al.* [7].

Figure 1 shows the pulse shape for the high foot experiments designed to produce the required high-adiabat radiation drive. The beginning of the pulse rises to  $\sim 40$  TW, the

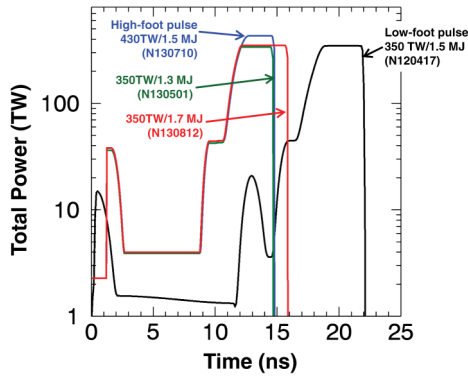


FIG. 1 (color online). Laser power vs time is shown for a representative low-foot pulse shape (black) and high-foot pulse shapes (N130710 in blue, N130501 in green, and N130812 in red). The salient features of the high-foot pulse shape are higher picket and trough powers and a shorter pulse duration, as well as the removal of the second laser impulse (seen in the low-foot case near 13 ns).

“picket”, then drops to  $\sim 3$  TW, the “trough”, which combined makes up the “high foot” of the pulse. A later  $\sim 40$  TW pulse launches the second shock, followed by the final, high-power, peak pulse. The high-foot implosions described in this Letter had peak pulse powers between 350 and 430 TW and total laser energies between 1.3 and 1.7 MJ. The laser pulse shape as well as the ratio of the power to the inner and outer beams (“cone fraction”) were optimized experimentally using surrogate capsules to tune the picket radiation symmetry [8] and shock timing [9] similar to what is done for low-foot implosions [10].

The capsule dimensions, silicon dopant levels, and profiles were the same as those used for the low-foot designs [2]: the inner capsule radii were  $935 \pm 8 \mu\text{m}$  and the ablator thickness were  $195 \pm 3 \mu\text{m}$  at cryogenic temperatures. The silicon doped ablaters had five layers of

graded density CH plastic to give a favorable Atwood number during the acceleration phases of the implosion. The DT ice layer thickness was  $69.0 \pm 1.2 \mu\text{m}$ .

Near the time of implosion stagnation (bang time), the hot spot shapes of the x-ray emissions were imaged by time resolved framing cameras [11] from both the equatorial view and the polar view. The equatorially mounted neutron imaging system (NIS) [12] provided images of the nuclear burn region from both direct (13–17 MeV) neutrons and down-scattered neutrons (6–12 MeV). The DT fusion yield was measured by neutron time-of-flight detectors (NTOFs) [13], nuclear activation detectors (NADs) distributed around the NIF target chamber [14], and the magnetic recoil spectrometer (MRS) [15]. The yield values reported here are weighted averages of all the measurements. The  $T_{\text{ion}}$  is measured from the observed thermal broadening of the energy spectra as determined by the NTOF detectors for both the DT and DD neutron reactions. The neutrons between 10 and 12 MeV detected by the NTOFs and MRS are from the neutrons that scattered off of the fuel. The down-scattered ratio (DSR) is defined to be the ratio of the number of neutrons from 10 to 12 MeV to the number between 13 to 15 MeV. It is related to the fuel  $\rho R$  by  $\rho R [\text{g}/\text{cm}^2] = 20.4 \times \text{DSR}$  from the consideration of implosion geometry and neutron ranges [15].

A total of five high-foot cryogenically layered implosions were performed as of August 13, 2013. Four of these shots used a nominal dimension hohlraum, 5.75 mm in diameter, 9.4 mm long, with a 3.1 mm diameter laser entrance hole. One of these shots used a different length (10.1 mm) hohlraum and another had a far out-of-tolerance DT ice layer—these two shots are not discussed here, but will be included in a future paper. Table I summarizes the performance of the other three high-foot implosions along with the results of a 2D hohlraum simulation of N130812.

TABLE I. Summary of experimentally measured performance parameters from the three high-foot shots.

	N130501	N130710	N130812	Simulation for N130812
Laser energy (MJ)	1.292	1.484	1.693	input
Peak power (TW)	353.7	433.9	354.9	input
Coasting time (ns)	2.1	1.8	0.9	input
DT yield (13–15 MeV)	$7.67 \pm 0.16 \times 10^{14}$	$1.05 \pm 0.02 \times 10^{15}$	$2.40 \pm 0.05 \times 10^{15}$	$3.54 \times 10^{15}$ ( $\alpha$ on) $2.04 \times 10^{15}$ (no- $\alpha$ )
$T_{\text{ion}}$ (DT) (keV) (NTOF)	$3.0 \pm 0.13$	$3.5 \pm 0.13$	$4.2 \pm 0.16$	2.95
$T_{\text{ion}}$ (DD) (keV) (NTOF)	$2.7 \pm 0.2$	$3.2 \pm 0.2$	$3.7 \pm 0.2$	2.8
DSR (%)	$2.96 \pm 0.19$	$3.30 \pm 0.20$	$4.21 \pm 0.31$	3.27
Bang time (ns) ( $\gamma$ )	$16.76 \pm 0.03$	$16.46 \pm 0.05$	$16.75 \pm 0.03$	16.62
Burn width (ps) ( $\gamma$ )	$172 \pm 40$	$180 \pm 40$	$156 \pm 30$	160
$P_0$ ( $\mu\text{m}$ ) (x-ray)	$25.6 \pm 4.6$	$39 \pm 1.4$	$37.4 \pm 2.0$	34.1
$P_2/P_0$ (x-ray)	$12.1 \pm 9.2\%$	$-37 \pm 7.3\%$	$-24 \pm 3.4\%$	-23%
$M_0$ ( $\mu\text{m}$ ) (x-ray)	$33.7 \pm 1.7$	$50.2 \pm 1.7$	$44.7 \pm 1.8$	40
Mix mass (ng)	24	41	$\sim 0$	
Velocity (km/s)	296	337	312	312
YOC 1D	60%	35%	68%	
$P$ (Gbar)	81	53	108	110

The coast time (the time between when the laser is turned off and bang time) is also noted in Table I. The laser power remained on until the capsule has converged to  $\sim 300 \mu\text{m}$  diameter for N130812, corresponding to a coast time of  $\sim 1$  ns. The laser drive beyond this time is expected to be ineffective as the capsule is too small to effectively absorb the x-ray energy to further compress. The level of mix mass is inferred from the elevated x-ray yields due to higher  $Z$  ablator mixing into the hot spot above the calculated clean hot spot emission [16]. For the shots in this high-foot campaign, the inferred mix mass was  $< 200$  ng indicating very low mix from the RM and RT instabilities, confirming one of the key goals of the campaign. The peak fuel implosion velocities are not directly measured; instead they are scaled from “convergent ablator” [17] experiments that provide images of the convergence of  $D^3$  He gas-filled capsule surrogates under the same high-foot first and second shock pulses. The YOC (experimental DT yield in the 13–15 MeV range over the 1D simulation DT yield including  $\alpha$ -particle self-heating) for N130812 is close to 70%. The implosion stagnation pressure is calculated from the measured fuel  $\rho R$ ,  $T_{\text{ion}}$ , and constructed hot spot volume [18].

X-ray and neutron images of the hot spot for N130812 are shown in Fig. 2. The equatorial shape is oblate with double lobed features and the polar view shows a toroidal shape. Post-shot 2D axisymmetric HYDRA [19] simulations (bottom row) show similar shape and sizes. The equatorial  $\{r_p(\theta) = P_0[1 + (P_2/P_0)P_2(\cos(\theta)) + \dots]\}$  and polar  $\{r_m(\theta) = M_0[1 + (M_2/M_0)\cos(\theta) + \dots]\}$  Legendre and Fourier modes, summarized in Table I, show that N130501 had the roundest hot spot shape. N130710, at higher laser power, became more oblate in the equatorial ( $P$ ) view and

displaying an obvious toroidal shape in the polar ( $M$ ) view. On NIF, the  $M$  modes are introduced from the azimuthally asymmetric laser illumination on the inside of the hohlraum wall. N130812 used the same laser power as N130501, but over a longer time to reduce “coasting.” N130812 achieved very high performance with improved hot spot shape over N130710, but still obviously toroidal. The toroidal shape is likely a consequence of a known  $P_4$  mode that is imposed on the ablator due to the beam pointing on the hohlraum wall [10]. The oblate shape may be due to restricted inner beam laser propagation at late time that slightly cools the radiation drive at the waist of the implosion as compared to the poles. While the shapes are not spherical, the surface to volume ratio of the observed hot spot shapes and pressures are not that different from those expected of a round hot spot. In addition, analysis indicate that the implosion performance is not degraded significantly until  $|P_2/P_0| > 20\%$ . So for modest departures from spherical symmetry, a 1D model scan reasonably predicts the yield performance.

On shots N130501 and N130710, the measured and simulated  $T_{\text{ion}}$ 's are in fair agreement in both the DD and DT channels, while on N130812, the  $T_{\text{ion}}$  of 4.2 keV was higher than the simulations by several hundred eV and significantly different from the  $\sim 3.7$  keV inferred from the DD signal. Some difference,  $\sim 200$ – $300$  eV, between the DD and DT inferred  $T_{\text{ion}}$  is expected because of the differences in slopes of the DD and DT fusion reaction rates as a function of temperature—spreads in  $T_{\text{ion}} > 300$  eV are harder to understand. The higher than expected  $T_{\text{ion}}$ , may partially be attributable to motional broadened, but may also be a reflection of conductivity model uncertainties or

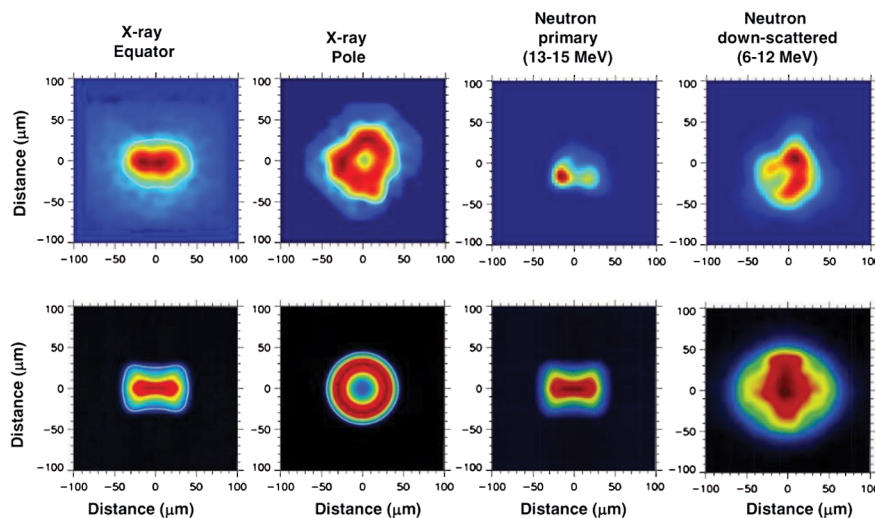


FIG. 2 (color online). Hot spot and down-scattered images from cryogenic layered DT implosion shot N130812. From left-to-right, the figure shows x-ray images of emission intensity in the equatorial and polar view, and neutron images in the equatorial view for direct (13–15 MeV) neutrons, and down-scattered (6–12 MeV) neutrons. The color scale reflects emission intensity [red (dark gray) is high intensity, blue (light gray) is low]. The upper row shows the images from the experiment, and the lower row shows results from post-shot 2D HYDRA simulations. Notably, both experiment and simulation showed oblate x-ray hot spot images viewed from the equator and a toroidal shaped hot spot when viewed from the pole.

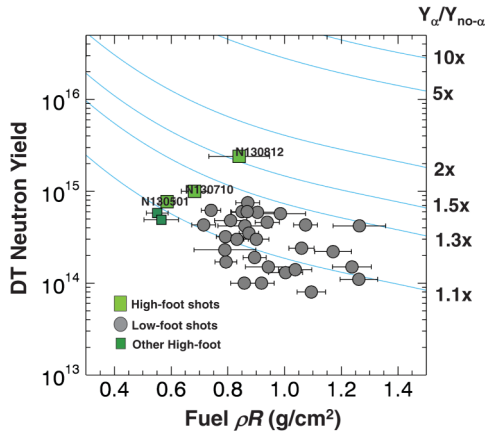


FIG. 3 (color online). A scatter plot of total DT neutron yield versus fuel areal density  $\rho R$  ( $g/cm^2$ ) for cryogenic layered DT implosions on NIF for the low-foot series (gray circles) and high-foot series (green squares). Contours of  $\alpha$ -heating multiplication are shown as the blue curves. The shots that are the discussed in this Letter are labeled by shot number: N130501, N130710, and N130812. A key point to note is that shot N130812 achieved a 50% boost in neutron yield due to  $\alpha$ -particle heating of the hot spot, as denoted by  $Y_\alpha/Y_{no-\alpha} \sim 1.5$ .

lower than expected fuel adiabat (which would be consistent with the observed DSR).

Figure 3 shows the experimental DT yield versus fuel areal density for the high-foot campaign (green squares) and previous low-foot implosions (gray circles). The first shot of the series, N130501, outperformed previous low-foot shots in total yield, but had lower fuel  $\rho R$ , consistent with the higher adiabat created by the high-foot design. The high-foot implosions reside in the upper left region of Fig. 3, illustrating the trade off of between compression

(towards higher  $\rho R$ ) and higher neutron yield. Contours of the ratio of yield with and without  $\alpha$ -particle energy deposition ( $Y_\alpha/Y_{no-\alpha}$ ) are noted.

N130812 produced more neutrons than the preshot predictions from 1D simulations without including  $\alpha$ -particle energy deposition. This suggests that  $\alpha$ -particle self-heating augmented the total DT neutron yield in the experiment.  $\alpha$ -particle self-heating is a necessary condition for ignition as it is the key mechanism that deposits fusion energy back into the fusion fuel, creating the necessary boot strapping of temperature and the creation of yet more  $\alpha$  particles [20]. The hot spot and  $\alpha$ -particle self-heating condition can be obtained from the measurements on N130812, without relying upon simulations [21]. From the shape measurements, we calculate the hot spot volume,  $V_{hs} = (2.3 \pm 0.04) \times 10^5 \mu m^3$  and equivalent spherical radius  $r_{hs} = (37.8 \pm 2) \mu m$ . The total neutron yield of  $2.84 \times 10^{15}$  is derived from the measured 13–15 MeV yield and the DSR by using the relation of:  $Y_{tot} = Y_{13-15} e^{4 \cdot DSR}$ . This is equivalent to an energy of  $E_{fusion} = 8$  kJ. From the measured  $T_{ion} = 4.2$  keV, neutron burn width,  $\tau_n = 156$  ps, and  $V_{hs}$ , we use standard formula's for the DT reaction rate [22] to calculate the yield in terms of an unknown number density  $n$  that can be solved for finding  $n = (6.7-8.4) \times 10^{24} cm^{-3}$  and mass density  $\rho_{hs} = (27.5-35.1) g/cm^3$ . One can then construct the hot spot areal density ( $\rho R_{hs} = (0.10-0.13) g/cm^2$ ) and hot spot energy ( $E_{hs} = (3.13-3.53)$  kJ). The fraction of  $\alpha$ -particle energy deposited into the hot spot can be calculated from  $\rho R_{hs}$  and  $T_{ion}$  [23] finding (0.72–0.77)—the  $\alpha$ -particle energy deposited can then be found from this fraction and  $E_{fusion}$  obtaining  $E_\alpha = (1.08-1.24)$  kJ. Thus,  $E_\alpha/E_{hs} = (0.34-0.35)$  supporting our assertion of significant  $\alpha$ -particle self-heating.

Figure 4(a) shows the measured yields of cryogenic DT implosions on NIF plotted against the yield expected

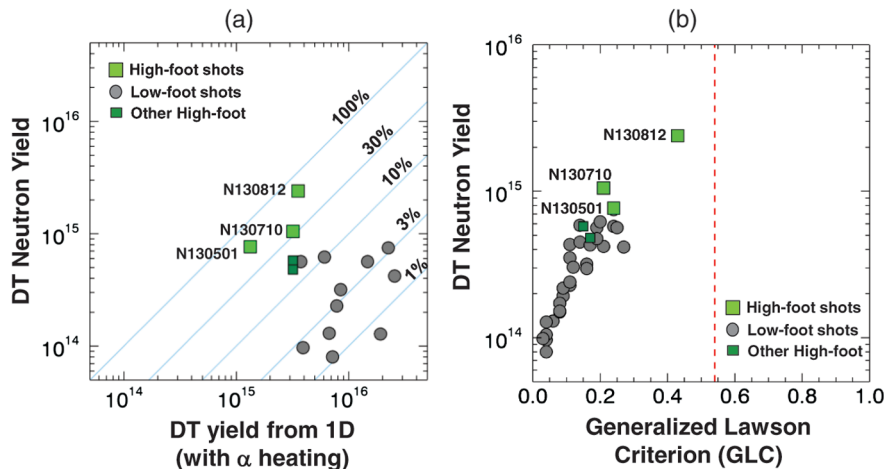


FIG. 4 (color online). Plots of observed neutron yield versus simulation and GLC. (a) The total experimentally determined yield (vertical axis) versus the yield predicted from 1D simulations (horizontal axis). The diagonal blue lines show contours of experimental yield over clean (YOC) 1D simulation which include  $\alpha$  heating. (b) The experimentally observed DT neutron yields vs the generalized Lawson criterion. Notably, shot N130812 reached  $GLC \sim 0.43$ . The vertical dashed line at  $GLC = 0.54$  corresponds to the threshold of  $Y_\alpha/Y_{no-\alpha} = 2$ , corresponding to a yield doubling due to  $\alpha$  heat deposition in the hot spot.

from the 1D simulation. The high-foot shots have higher absolute performance and higher YOC. Figure 4(b) is the DT yield vs the generalized Lawson criterion (GLC). The GLC [24,25] is a metric for gauging the performance of ignition capsule designs and is defined to be the condition where the fusion energy production rate is equal to the plasma loss. The GLC can be written as:

$$\text{GLC}(\chi) = \left[ \frac{\rho R}{1.5} \left( \frac{T_{\text{ion}}}{3.8} \right)^{2.2} \right]^{0.8} \quad (1)$$

The GLC is closely related to the  $\alpha$  particle deposited internal energy in the hot spot compared to the work necessary to compress the hot spot through a change in volume. A GLC of  $\chi = 0.54$  is required for a yield doubling due to  $\alpha$ -particle self-heating. The values of the GLCs for the series of shots N130501, N130710, and N130812 are  $\chi = 0.24, 0.21, \text{ and } 0.43$ , respectively.

In conclusion, the performance of indirectly driven, cryogenic DT layered implosions using a high-foot, higher adiabat design has been measured, and the results have been very encouraging. In particular, these high-foot implosions have generated YOC >50%, bringing experiment and simulations into closer agreement; DT neutron yields >10<sup>15</sup> in cryogenic layered implosions for the first time; and a 50% yield boost due to  $\alpha$  heating, another first. The comparison with the low-foot, low-adiabat series of implosions is interesting and instructive. The high-foot series used a shorter, three-shock drive with a higher foot, and produced a higher fuel adiabat, higher yields, less hot spot mix, but modest fuel areal densities. The low-foot series of implosions used a longer, four-shock drive, and produced a lower fuel adiabat, lower yields, higher hot spot mix, but higher fuel areal densities [2,3,4]. Creating a higher adiabat and higher radiation temperature early in the drive appears to be an effective means for reducing hot spot mix by reducing ablation front RM and RT instability growth. Future work will focus on avenues for increasing the fuel velocity and areal density while holding ablation-front RT growth and hot spot mix under control, to approach the conditions required for ignition [21].

We would like to thank the entire NIF operations, cryogenics, diagnostics, and target teams. We would also like to thank Dr. P. Albright, Dr. J. Atherton, Dr. M. J. Edwards, Dr. J. Lindl, Dr. E. Moses, Dr. C. Verdon, and

Dr. A. Wan for their support. This work was performed under the auspices of the U.S. Department of Energy by Lawrence Livermore National Laboratory under Contract No. DE-AC52-07NA27344.

\*park1@llnl.gov

†hurricane1@llnl.gov

- [1] J. D. Lindl and E. I. Moses, *Phys. Plasmas* **18**, 050901 (2011).
- [2] S. W. Haan *et al.*, *Phys. Plasmas* **18**, 051001, (2011).
- [3] M. J. Edwards *et al.*, *Phys. Plasmas* **18**, 051003 (2011).
- [4] M. J. Edwards *et al.* *Phys. Plasmas* **20**, 070501 (2013).
- [5] S. E. Bodner, *Phys. Rev. Lett.* **33**, 761 (1974).
- [6] V. Goncharov and O. A. Hurricane, LLNL Report No. LLNL-TR-562104, 2012; LLNL Report No. LLNL-TR-570412, 2012.
- [7] T. R. Dittrich, O. A. Hurricane, D. A. Callahan, E. L. Dewald, T. Döppner, D. E. Hinkel, L. F. Berzak Hopkins, S. Le Pape, T. Ma, J. L. Milovich, J. C. Moreno, P. K. Patel, H.-S. Park, B. A. Remington, J. D. Salmonson, and J. L. Kline, following Letter, *Phys. Rev. Lett.* **112**, 055002 (2014).
- [8] E. Dewald *et al.*, *Phys. Rev. Lett.* **111**, 235001 (2013).
- [9] H. F. Robey *et al.*, *Phys. Rev. Lett.* **108**, 215004 (2012).
- [10] O. L. Landen *et al.*, *Phys. Plasmas* **18**, 051002 (2011).
- [11] P. M. Bell *et al.*, *Rev. Sci. Instrum.* **81**, 10E540 (2010); S. Glenn *et al.*, *Rev. Sci. Instrum.* **81**, 10E539 (2010).
- [12] F. E. Merrill *et al.*, *Rev. Sci. Instrum.*, **83**, 10D317 (2012); G. P. Grim *et al.*, *Phys. Plasmas* **20**, 056320 (2013).
- [13] V. Yu. Glebov *et al.*, *Rev. Sci. Instrum.* **77**, 10E715 (2006).
- [14] D. L. Bleuel *et al.*, *Rev. Sci. Instrum.* **83**, 10D313 (2012).
- [15] M. Gatu Johnson *et al.*, *Rev. Sci. Instrum.* **83**, 10D308 (2012).
- [16] T. Ma *et al.*, *Phys. Rev. Lett.* **111**, 085004 (2013).
- [17] D. G. Hicks *et al.*, *Phys. Plasmas* **19**, 122702 (2012); D. G. Hicks, B. K. Spears, D. G. Braun, R. E. Olson, C. M. Sorce, P. M. Celliers, G. W. Collins, and O. L. Landen, *Rev. Sci. Instrum.* **81**, 10E304, (2010).
- [18] C. Cerjan, P. T. Springer, and S. M. Sepke, *Phys. Plasmas* **20**, 056319 (2013).
- [19] M. M. Marinak, G. D. Kerbel, N. A. Gentile, O. Jones, D. Munro, S. Pollaine, T. R. Dittrich, and S. W. Haan, *Phys. Plasmas* **8**, 2275 (2001).
- [20] G. S. Fraley, E. J. Linnebur, R. J. Mason, and R. L. Morse, *Phys. Fluids* **17**, 474 (1974).
- [21] O. A. Hurricane *et al.*, Lawrence Livermore National Laboratory Report No. LLNL-JRNL-645169, 2013.
- [22] H.-S. Bosch and G. M. Hale, *Nucl. Fusion* **32**, 611 (1992).
- [23] O. N. Krokhin and V. B. Rozanov, *Sov. J. Quantum Electron.* **2**, 393 (1973).
- [24] C. D. Zhou and R. Betti, *Phys. Plasmas* **16**, 079905 (2009).
- [25] B. K. Spears *et al.*, *Phys. Plasmas* **19**, 056316 (2012).